# Iodide⋯π interactions of perhalogenated quinoid rings in co-crystals with organic bases*

*Krešimir Molčanov[a], Gregor Mali[b], Jože Grdadolnik[b], Jernej Stare[b], Vladimir Stilinović[c], Biserka Kojić-Prodić[a]*

a Rudjer Bošković Institute, Bijenička 54, Zagreb HR-10000, Croatia

b National Institute of Chemistry, Hajdrihova 19, Ljubljana, SI-1000, Slovenia

c Department of Chemistry, Faculty of Science, University of Zagreb, Horvatovac 102a, Zagreb HR-10000, Croatia

*Dedicated to prof. Dietmar Stalke on occasion of his 60th birthday.

KEYWORDS charge transfer, quinone, semiquinone radical, solid-state NMR, IR spectroscopy, crystal structure, anion⋯π interactions, DFT calculations.

ABSTRACT First anion⋯π contacts with quinoid rings have been described in novel co-crystals of tetrabromo- and tetrachloroquinone with iodide salts of substituted *N*-methylpyridinium

cations. In seven crystal structures of these co-crystals a centrosymmetric unit I⁻···quinone···I⁻ is observed involving close contacts between iodide anions and electron-depleted carbon skeletons of the quinoid rings. However, the salt with *N*-methyl-4-methylcarboxypyridinium base crystallizes in two polymorphs characterized by O=C···quinone···C=O interaction instead of I⁻ ···quinone···I⁻ one. A possible charge transfer, suggested by black color of the crystals, is probed by solid-state NMR and IR spectroscopies and analyzed by DFT calculations.

INTRODUCTION

Among intermolecular interactions of π-electron system anion···π interactions are the least common.[1] Since the aromatic ring is electron rich, it typically participates in π-stacking[2-5] and C-H···π interactions;[6,7] cation···π contacts formed between aromatic rings and large, polarizable cations ("soft" cations) are also common.[8] A close contact with an anion or a lone electron pair is possible for electron-depleted rings and a number of such interactions have been documented.[9-16]

Unlike aromatics, which are mostly electron-rich (except those with five or six electron-withdrawing substituents), quinoid rings are inherently electron-poor due to a lack of electron delocalization and the presence of carbonyl groups; they can be further depleted by introduction of electronegative substituents. Perhalogenoquinones act as mild oxidants and can easily be reduced into semiquinone radicals by mild reducing agents such as iodide ions.[17] Due to their extreme electron depletion,[18] they may be expected to form anion···π interactions.

While preparing solid-state semiquinone systems,[17,19-22] we serendipitously obtained a series of co-crystals of tetrachloro- and tetrabromoquinone (Cl$_4$Q and Br$_4$Q, respectively, Scheme 1) with iodide salts of organic cations (mostly derivatives of *N*-methylpyridinium, Scheme 2), in which close contacts between the quinoid ring and the iodide anion occur almost without exception.

These contacts play a major role in crystal packing, however, the most intriguing part is charge transfer, which may be obvious from color change of the crystals. In this paper we present crystal structures of the first co-crystals of Cl₄Q and Br₄Q with organic iodides and describe for the first time observed charge transfer through an anion···π interaction.
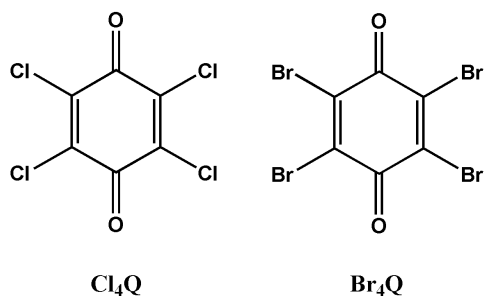


**Scheme 1** Quinones used in the preparation of co-crystals.
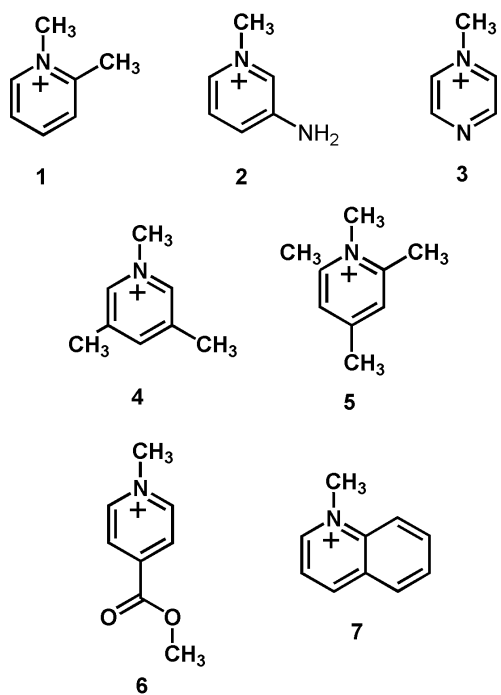


**Scheme 2** Cations of organic iodides used in the preparation of co-crystals: *N*-methyl-2-picolinium (**1**), *N*-methyl-3-aminopyridinium (**2**), *N*-methylpyrazinium (**3**), *N*-methyl-2,5-

dimethylpyridinium (**4**), *N*-methyl-2,4,6-trimethylpyridinium (**5**), *N*-methyl-4-methylcarboxypyridinium (*N*-methylisonicotinic acid methyl ester, **6**), *N*-methylquinolinium (**7**).

RESULTS AND DISCUSSION

All eight prepared ionic co-crystals have a stoichiometry of two formula units of the organic iodide and one quinone molecules: $1_2 \cdot Br_4Q$, $2_2 \cdot Br_4Q$, $3_2 \cdot Br_4Q$, $4_2 \cdot Br_4Q$, $5_2 \cdot Br_4Q$, $6_2 \cdot Br_4Q$ (two polymorphs, monoclinic and triclinic), $7_2 \cdot Br_4Q$ and $7_2 \cdot Cl_4Q$ (numbers in bold correspond to organic bases in Scheme 2).

*Structure/property correlations: Color/electronic structure and morphology of the crystals/crystal packing*

Oxidation state of quinoid compounds is correlated to their color: neutral quinones $Cl_4Q$ and $Br_4Q$, are yellow (Fig. 1a), whereas the salts of their radical anions are black or very dark red (Fig. 1b). The studied ionic co-crystals, which formally comprise a neutral quinone and an iodide salt of an organic cation, are also black or very dark red (Fig. 1c). All organic iodide salts used in preparations were either white or pale yellow. Therefore, black color of the studied co-crystals can only be a result of charge transfer; a partial charge transfer from the iodide anion to the quinone molecule can be expected.

While iodide co-crystals and semiquinone radical salts have the same color, morphology of the crystals are rather different. All salts of the semiquinone radical[17,19-21,23,24] crystallize as needles and comprise infinite π-stacks of the radicals; the needles are elongated in the direction of stacking (Fig. 1b). This indicates that π-stacking of radicals is the strongest intermolecular interaction in their salts. Morphologies of iodide co-crystals vary considerably: some are plate-

like, others are prismatic (Fig. 1c). Indeed, infinite π-stacking typical of semiquinone radicals is not detected in the series studied in this work (see below).

In the sample of $3_2 \cdot Br_4Q$ that the plate-like ionic co-crystals form first; in a solution left overnight in sealed vessel, these co-crystals decomposed, and needle-like crystals of radical salts were grown.[25] The reaction indicates that the formation of the iodide co-crystals is a kinetically controlled process, whereas the radical salts are thermodynamically more stable.
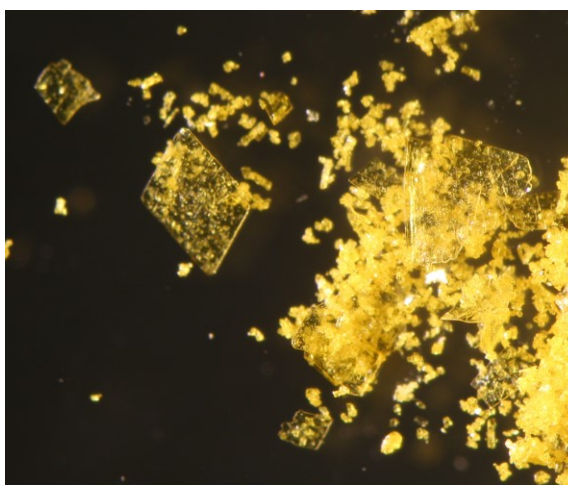


a)
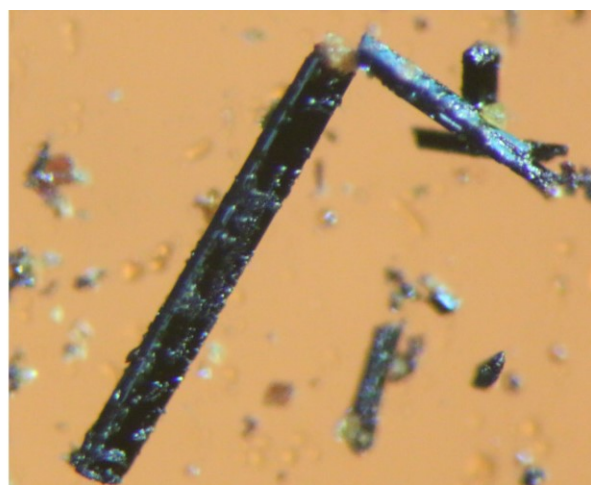
b)
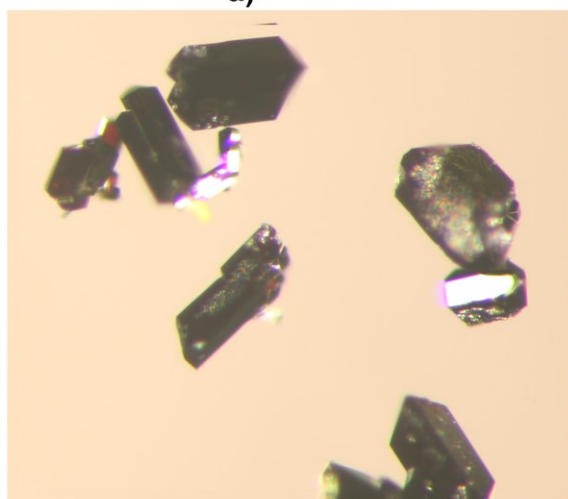
c)
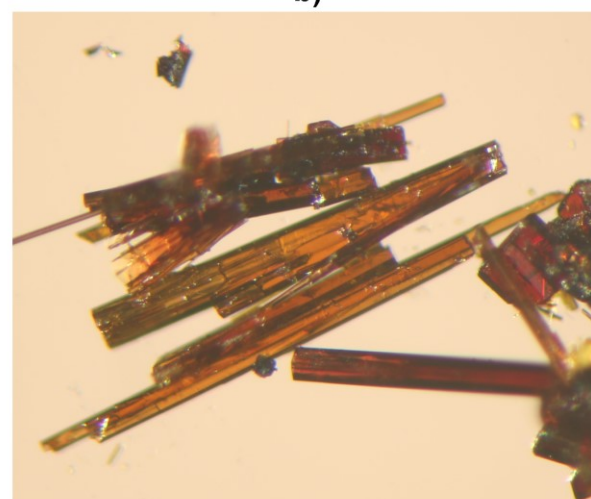
d)

**Figure 1** Crystals of studied compounds: a) neutral Br$_4$Q, b) *N*-methylpyridinium salt of Br$_4$Q anion radical [21], c) a co-crystal of Br$_4$Q with *N*-methyl-3,5-dimethylpyridinium iodide (**3**$_2$·Br$_4$Q) and d) co-crystals of Br$_4$Q with *N*-methyl-4-methylcarboxypyridinium (**6**$_2$·Br$_4$Q) with both polymorphs present.

*Crystal packing and close iodide-quinone contacts*

In all studied ionic co-crystals, except **6**$_2$·Br$_4$Q, the basic unit I$^-$···quinone···I$^-$ occurs: two iodide ions form close contacts with a quinoid ring in a "sandwich-like" fashion (Fig. 2). These contacts involve iodide-carbon distances shorter than the sum of van der Waals radii (3.76 Å); charge transfer between the iodide anion and the quinoid ring may be possible, and this would explain the black color of the crystals. Indeed, crystals of both **6**$_2$·Br$_4$Q polymorphs lacking I$^-$ ···quinone···I$^-$ unit, are light brown and transparent (Fig. 1d).

In these structures the quinone and the corresponding I$^-$···quinone···I$^-$ units are centrosymmetric, with a single symmetry-independent close contact. To describe geometry of the close contacts, we defined the following geometric parameters: distance between the ring centroid and the iodide anion, *d*(Cg), distance between the ring mean plane and the iodide anion, *d*(plane), angle between the ring plane and *d*(Cg), α, and direction of the offset relative to the molecular axis O=C···C=O, β (Fig. 3). Offset can be calculated as *d*(Cg)·cos α. Geometric parameters of the close contacts between the quinoid rings and iodide anions are listed in the Table 1. The I$^-$···quinone···I$^-$ units reveal the anion offset along the O=C···C=O direction typically by 0.8 - 1.5 Å (α angles are less than 20°, Fig. 3) resulting in close contacts between the iodide and C atoms (Table S3), of which carbonyl C is the most electron-depleted one (Fig. 4).

Analysis of Hirshfeld surfaces and electrostatic potential reveals that the carbon skeleton has considerable positive potential (Fig. 4a), which indicates attractive interactions between the ring and the iodide anions. The central part of the quinoid ring is slightly depressed, making the contact area between the carbon skeleton and the iodide anion larger. This effect is even more pronounced in Voronoi-Dirichlet polyhedra (Fig. 4b). While the depression consists of six small faces, the total area represents 5 - 10 % of the total molecular VDP surface. Since size of a VDP face is approximately proportional to the energy of the interaction,[26] these quinone···I$^-$ interactions cannot be neglected as justified by DFT calculations presented in this work.

Crystal packings of $1_2$·Br$_4$Q - $5_2$·Br$_4$Q, $7_2$·Br$_4$Q and $7_2$·Cl$_4$Q are characterized by I$^-$ ···quinone···I$^-$ units and cations involved in polar contacts. In two polymorphs of $6_2$·Br$_4$Q there are close contacts between carbonyl oxygen of the methoxycarboxyl group of the cation and the quinoid π-system. This very contact is the n→π* interaction occuring between lone pair of carbonyl group and π-system.[14] It is dominated by the electron delocalisation of a lone pair from a carbonyl oxygen and an empty antibonding π* orbital. A signature of this interaction would be that iodine points towards to one of carbonyls rather than to the centroid of the ring (Fig. 5a). Sandwich-like carbonyl···quinone···carbonyl moieties are formed (Fig. 5), which which play an analogous role in crystal packing to I$^-$···quinone···I$^-$ units observed in other compounds (Fig. 5). Iodide ions are involved in C-H···I hydrogen bonds and C-Br…I$^-$ contacts. Crystal packing of two polymorphs of of $6_2$·Br$_4$Q are essentially close packings of carbonyl···quinone···carbonyl motifs and iodide anions (Figs. 5b and S23).

The iodides additionally participate in halogen bonding with the neighbouring Br$_4$Q molecules. Neutral Br$_4$Q is a respectable halogen bond donor as evidenced by the regions of positive ESP on bromine atoms (generally referred to as σ-holes, Fig. 4), and also by partial charge on the

bromine of +0.153 e, which implies $Br_4Q$ is a somewhat stronger halogen bond donor than the 'classical' 1,4-dibromotetrafluorobenzene[27] (+0.149 e), and weaker than *N*-bromoimides (+0.18 - +0.2 region).[28,29] As a result, generally all four bromine atoms of each $Br_4Q$ molecule form halogen bonds with iodide anions (halogen bond lengths between 3.42 Å and 3.70 Å), the only exception being $4_2 \cdot Br_4Q$, where only two bromine atoms participate in halogen bonding. Each iodide on the other hand acts as an acceptor of two halogen bonds (again $4_2 \cdot Br_4Q$ being the only exception, with only one halogen bond per iodide), with the angle between the two halogen bonds between 90° and 120°. Similar bent geometry has been described in numerous structures of organic halogen[30] and hydrogen[31] bonded organic halides, and have been explained by the polarization of the halide upon forming a non-bonding interaction – the electron density in the continuation of the contact somewhat decreases, while it increases in a torus perpendicular to it. The second contact atom (i.e. a positive region of a halogen or hydrogen donor) then approaches the halide from the direction in which the negative charge on the halogen is maximal, i.e. at a 90° and 120° angle to the first one.

The most intriguing aspect of close iodide-π contacts is the apparent charge transfer. While it is common to estimate degree of charge transfer from molecular geometry,[32] in our case unfortunately results are inconclusive at best. Due to the presence of iodide ions and bromine atoms (high absorption), lengths of C-C and C-O bonds could not be determined with a sufficient accuracy, and structural correlation is not very reliable. Therefore, we decided to study the charge transfer by IR and solid-state NMR spectroscopy and theoretical quantum calculations based on the density functional theory (DFT) approach.
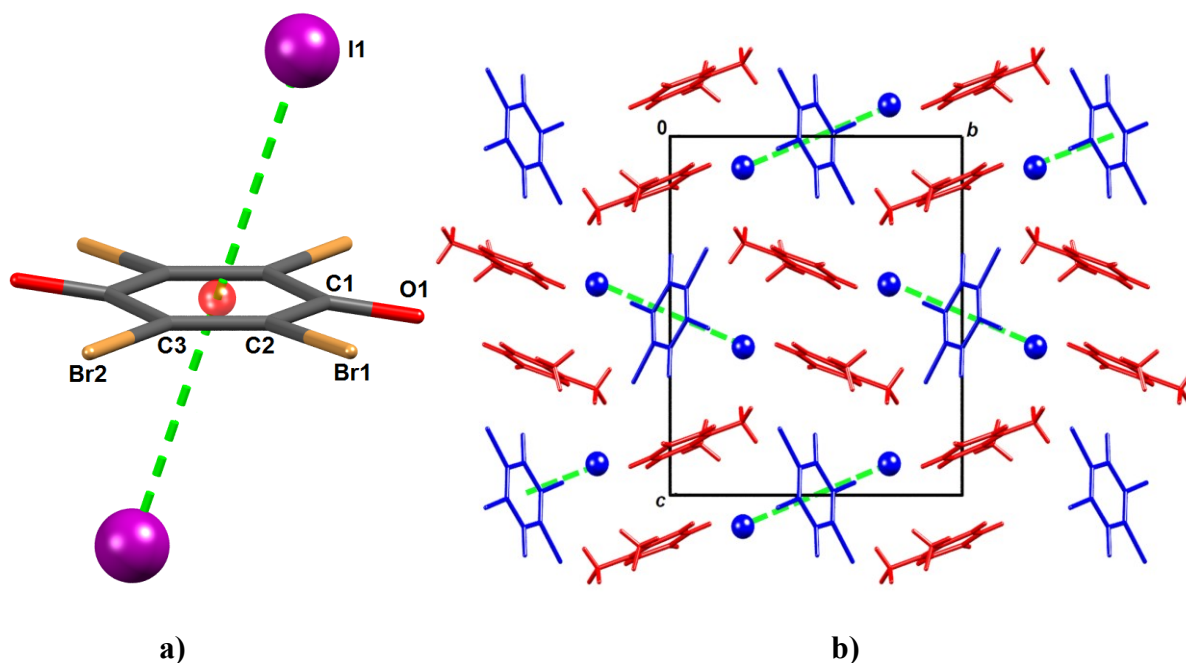
**Figure 2** a) The I⁻···quinone···I⁻ unit observed in all studied structures with exception of two polymorphs of **6₂**·Br₄Q. Atom numbering scheme applied to all structures is indicated; a centroid of the ring located at the crystallographic inversion centre is denoted by red sphere. b) Crystal packing of **1₂**·Br₄Q comprising I⁻···quinone···I⁻ units (blue) and *N*-methylpicolinium cations (red).
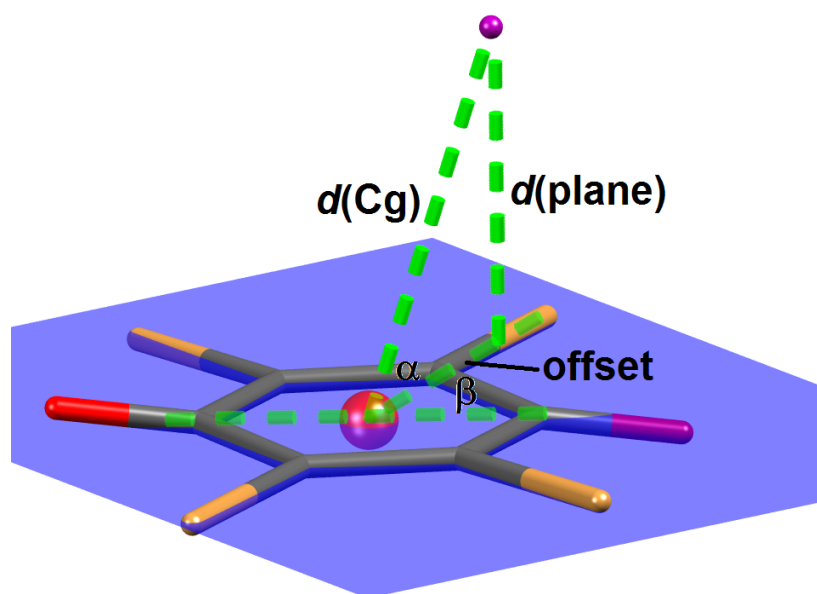
**Figure 3** Geometric parameters describing contact between a quinoid ring and an iodide anion. Cg is the centroid of the ring (red sphere), $d$(Cg) is distance between the iodide anion and ring centroid, $d$(plane) is the distance between the iodide anion and the mean plane of the quinoid ring, α is the angle between Cg⋯I⁻ line and ring plane, and β is an angle defining direction of offset. Offset can be calculated as $d$(Cg)·cos α.
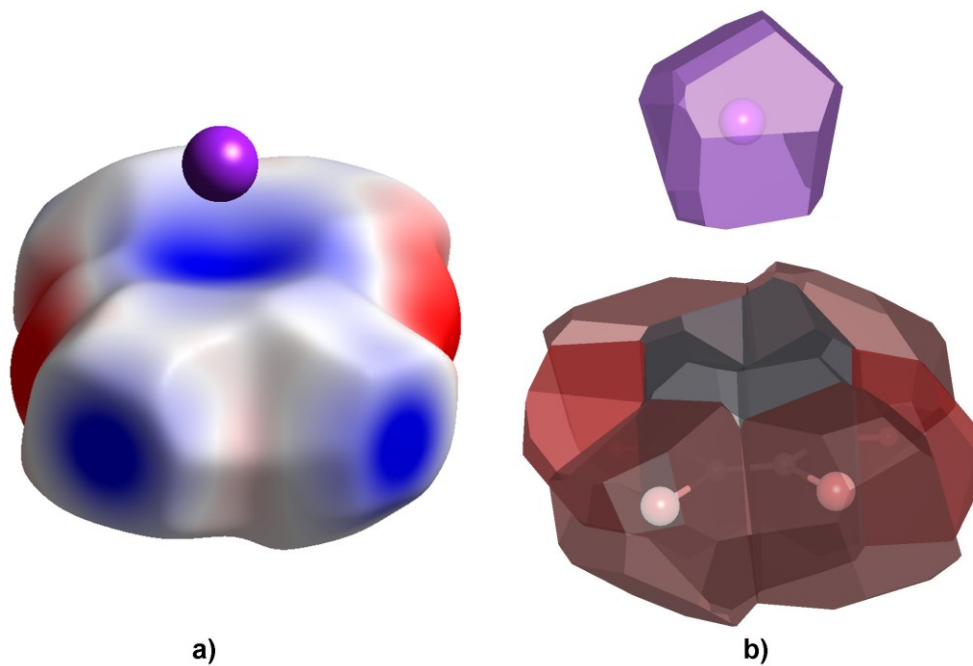
**Figure 4** a) Calculated electrostatic potential of a tetrabromoquinone molecule plotted onto a Hirshfeld surface (red: -0.04, blue +0.25 au) showing an electron-depleted quinoid ring and σ-holes on the bromine atoms; b) VDP polyhedra of the iodide (above) and $Br_4Q$ (below) in $1_2 \cdot Br_4Q$.
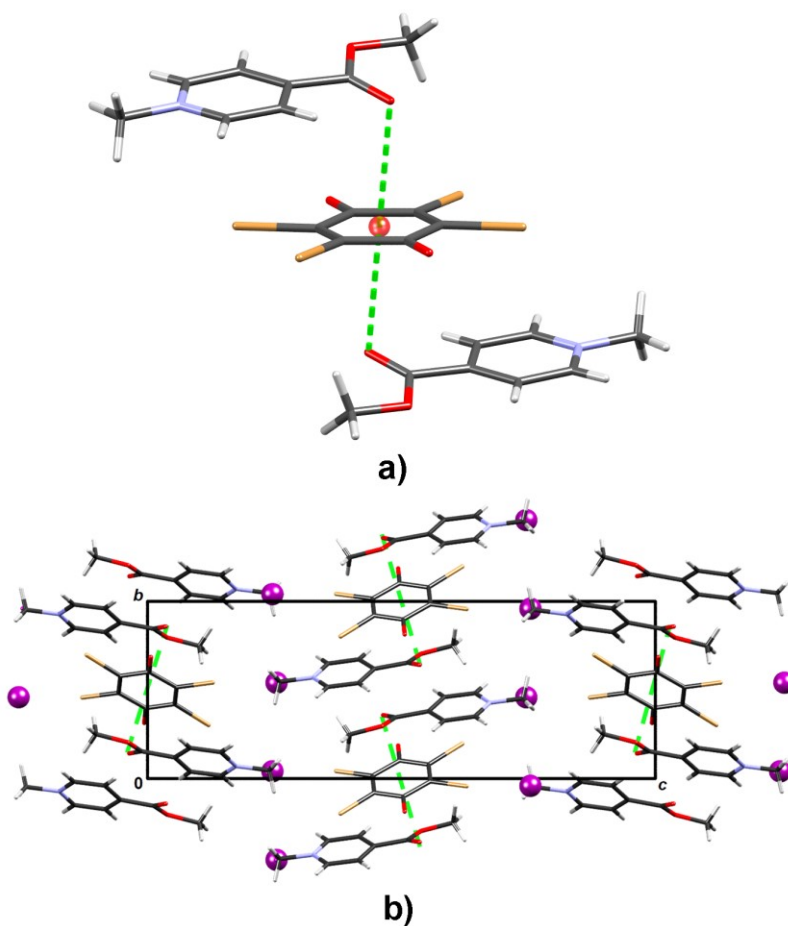
**Figure 5** a) The "sandwich-like" motif found in the two polymorphs of $6_2 \cdot Br_4Q$ formed by lone pair-π interaction: two carbonyl oxygens of methoxycarboxyl groups are in close contacts with π-system of a quinoid ring (a centroid denoted by a red sphere); b) crystal packing of monoclinic $6_2 \cdot Br_4Q$ with lone pair-π contact highlighted.

**Table 1** Geometric parameters of close contacts between iodide ions and quionid rings (Å, °), as defined in Fig. **3**.

| | $1_2 \cdot Br_4Q$ | $2_2 \cdot Br_4Q$ | $3_2 \cdot Br_4Q$ | $4_2 \cdot Br_4Q$ | $6_2 \cdot Br_4Q$, 100 K | $6_2 \cdot Br_4Q$, RT | $7_2 \cdot Br_4Q$ | $7_2 \cdot Cl_4Q$ |
|---|---|---|---|---|---|---|---|---|
| $d$(Cg) | 3.746 | 3.704 | 3.697 | 3.798 | 3.865 | 3.938 | 3.667 | 3.537 |

| d(plane) | 3.731 | 3.477 | 3.607 | 3.698 | 3.569 | 3.659 | 3.509 | 3.424 |
|---|---|---|---|---|---|---|---|---|
| α | 84.5 | 71.0 | 76.5 | 76.5 | 68.0 | 67.5 | 73.0 | 76.5 |
| β | 0.8 | 6.5 | 10.5 | 5.5 | 16.5 | 18.5 | 20.0 | 16.5 |
| offset | 0.94 | 1.22 | 0.91 | 0.36 | 1.20 | 0.86 | 0.88 | 1.45 |

*Solid-state NMR study of charge transfer*

Anticipating that an additional insight into the charge transfer between iodide anions and quinoid rings could be obtained by solid-state NMR spectroscopy, we recorded $^{13}$C NMR spectra of selected samples and compared these spectra to the $^{13}$C NMR spectra of $Br_4Q$ and $H_2Br_4Q$. The latter two solids exhibit very different carbon spectra. $Br_4Q$ shows two broad contributions, one belonging to C=O carbon nuclei resonating at *ca.* 170 ppm, and another belonging to C-Br carbon nuclei extending between 160 ppm and 125 ppm. The $^{13}$C NMR signals of $H_2Br_4Q$ are significantly shifted with respect to the signals of $Br_4Q$; C-OH nuclei resonate at *ca.* 146 ppm, and the broad contribution of C-Br extends between 140 ppm and 100 ppm. (The spectrum of $H_2Br_4Q$ shows also an additional signal at 166 ppm, which belongs to an unidentified impurity. Similar signals can be detected also in the $^{13}$C MAS spectra of other samples; see Figure S38.) According to the large chemical shift difference of the C=O and C-OH groups in $Br_4Q$ and $H_2Br_4Q$, one would expect that chemical shift of C=O carbon nuclei will be quite sensitive to the extent of charge transfer between iodide anions and quinoid rings in our materials. Unfortunately the measured spectra disprove that. The C=O signals of $1_2 \cdot Br_4Q$, $2_2 \cdot Br_4Q$, and $7_2 \cdot Br_4Q$ all resonate at 174 ppm, and the C=O signal of $4_2 \cdot Br_4Q$ resonates at 172 ppm. The spectra thus show that charge transfer does not significantly influence the chemical shift of the carbonyl carbon nuclei of the quinoid rings.

The above conclusion is, of course, based on the assumption that the signals resonating at about 170 ppm belong to carbonyl carbon nuclei of the quinoid rings. This assumption is supported by the ab-initio computations of $^{13}$C chemical shifts of the inspected materials. Figure S39 shows that the computed chemical shifts agree well with the measured chemical shifts of the C=O carbon nuclei and of the carbon nuclei within the $N$-methyl-2-picolinium (**1**), $N$-methyl-3-aminopyridinium (**2**), $N$-methyl-3,5-dimethylpyridinium (**4**), and $N$-methylquinolinium (**7**) cations. The assignment of all these signals is thus reliable. Oppositely, in all samples, even in the simple Br$_4$Q and H$_2$Br$_4$Q, the computations quite inaccurately predict chemical shifts of the C-Br carbon nuclei. This might be due to an inappropriate pseudopotential for bromine, as included within CASTEP and used in these calculations. Inappropriate pseudopotential could affect the prediction of electron density and consequently of chemical shifts in the close vicinity of bromine atoms.

In fact, it is very difficult to identify the signals of C-Br nuclei in **1**$_2$·Br$_4$Q, **2**$_2$·Br$_4$Q, **4**$_2$·Br$_4$Q and **7**$_2$·Br$_4$Q. Carbon NMR spectra of these samples in Figure 6 were measured with the $^1$H-$^{13}$C CPMAS approach, which enhances the signals of carbon nuclei with hydrogen nuclei in their neighborhood. It is thus not surprising that the C-Br signals cannot be seen, as they have no hydrogen nuclei close by. Figure S38 shows directly excited $^{13}$C MAS spectra of the same samples. As one can see, in spite of the long measurements, the signal-to-noise ratio of these spectra is rather low. Furthermore, whereas the signals of $N$-methyl-2-picolinium (**1**), $N$-methyl-3-aminopyridinium (**2**), $N$-methyl-3,5-dimethylpyridinium (**4**), and $N$-methylquinolinium (**7**) cations are relatively sharp, the C=O signals in **2**$_2$·Br$_4$Q, **4**$_2$·Br$_4$Q and **7**$_2$·Br$_4$Q are quite broad, similarly broad as the corresponding signal in Br$_4$Q. It can thus be expected that the C-Br signals are also smeared and as such more or less buried in the baseline of the spectra. The single

exception is the spectrum of $\mathbf{1}_2 \cdot Br_4Q$, in which the C=O signal is very sharp. Perhaps this is due to its different magnetic properties as compared to the properties of other inspected samples. In the spectrum of $\mathbf{1}_2 \cdot Br_4Q$, the signal of C-Br most probably resonates at 140 ppm; at least this signal is the strongest signal that cannot be assigned to *N*-methyl-2-picolinium (**1**) and that gets 'suppressed' by the CPMAS approach. As mentioned above, this is to be expected for the $^{13}C$ NMR signals of carbon nuclei that do not have hydrogen nuclei in their vicinity.
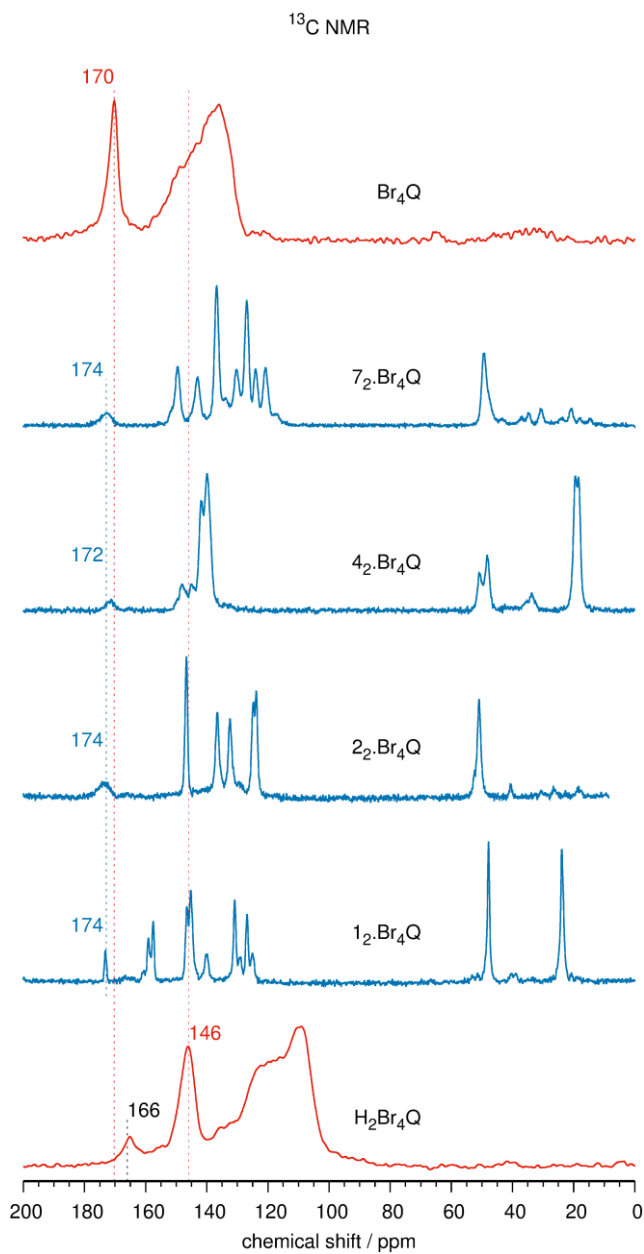
**Figure 6** $^{13}$C MAS NMR spectra of Br$_4$Q and H$_2$Br$_4$Q, and $^1$H-$^{13}$C CPMAS NMR spectra of **1**$_2$·Br$_4$Q, **2**$_2$·Br$_4$Q, **4**$_2$·Br$_4$Q and **7**$_2$·Br$_4$Q. ($^{13}$C MAS NMR spectra of **1**$_2$·Br$_4$Q, **2**$_2$·Br$_4$Q, **4**$_2$·Br$_4$Q and **7**$_2$·Br$_4$Q have significantly lower signal-to-noise ratio and are presented in Figure S38). Signals resonating at 170 ppm and more belong to carbonyl carbon nuclei of quinoid rings, and the signal resonating at 146 ppm belongs to C-OH nuclei of H$_2$Br$_4$Q. Weak signal at 166 ppm belongs to an unidentified impurity.

*IR spectroscopic study of the charge transfer*

The assignment of the most significant bands is presented in the Table 3. The fingerprint region in spectrum of pure $Br_4Q$ begins with structured band culminated at 1664 cm$^{-1}$. The origin of this band may be attributed to C=O stretching vibration. Two less intense but sharp bands surround the main peak at 1678 cm$^{-1}$ and 1640 cm$^{-1}$. The C=C-C ring vibration is attributed to complex band at 1542 cm$^{-1}$. Next intense band can be found at 1047 cm$^{-1}$ and is assigned to coupled C=C, and C-C stretchings and CCC and CCBr bending vibrations. Strong vibrational coupling is a common characteristic for all bands in the spectra of neutral compounds and co-crystals. The appearance of COH group in $H_2Br_4Q$ drastically changes the left side of the spectrum in the fingerprint region. The first sharp band of medium intensity appears at 1378 cm$^{-1}$ and is attributed to C-O-(H) stretching. The high frequency counterpart (OH stretching) can be found as a sharp peak located at 3389 cm$^{-1}$. The differences mainly in frequencies can be observed also for peaks that are associated with ring vibrations. The most prominent bands are thus located at 1450 cm$^{-1}$ and 1165 cm$^{-1}$.

The presence of cations significantly increases the complexity of the spectra of co-crystals. Strong overlapping between the $Br_4Q$ bands with those of cations screens the accurate assignment, especially in the region below 1500 cm$^{-1}$. Therefore the most accurate assigned are bands due to C=O stretching of carbonyls in bromanil molecule, which band frequency depends only slightly on the type of cation. **7** and **2** cations shift the C=O stretching to values found in neutral $Br_4Q$, while **1** and **4** blue shift C=O frequencies to 1672 cm$^{-1}$ and 1670 cm$^{-1}$, respectively. The prolongation of C=O bond may results in red shift of C=O stretch. Using the same approach the blue shift of C=O stretch may have origin in the shortening of the C=O bond length. However, we must have in mind that vibrational bands observed in spectra of probed co-crystals

are extremely coupled. This is true not only for ring vibrations but to some extend also for C=O stretch, which is at least partially coupled to various ring modes. Beside the change in bond length, the variation of the degree of coupling may also contribute to the frequency shifts of band which is predominately ascribed as C=O stretch. Calculation of PED for bromanil revealed that the band at 1664 cm$^{-1}$ contains only 85 % of C=O stretching mode.[33] Variation in coupling between C=O stretching and ring vibrations among different cations may be reason of lacking the correlation between the measured $d$(Cg···I)/Å and the C=O stretching frequency. Similar situation is observed in the case of C-Br stretching. This mode is coupled with various types of low frequency ring vibrations and extend of coupling may be cation depended. The variation in frequencies are quite pronounced but with no applicable correlation with $d$(Cg···I)/Å.

Described changes cannot be attributed to charge transfer phenomena. To clarify the predicted effect of charge transfer we have to emphasize that in the spectra of potassium salt of Br$_4$Q radical anion the C=O shifts to 1579 cm$^{-1}$,[33] which is still far away from the C-O stretch observed in H$_2$Br$_4$Q but significantly lower than in the case of probed co-crystals.

**Table 3** Assignment of the major absorption bands in the infrared spectra. Absorption bands of neutral Br$_4$Q[34] have been given for comparison.

| | Br$_4$Q[34] | H$_2$Br$_4$Q | N-MePy·Br$_4$Q | 1$_2$·Br$_4$Q | 2$_2$·Br$_4$Q | 4$_2$·Br$_4$Q | 7$_2$·Br$_4$Q |
|---|---|---|---|---|---|---|---|
| $d$(Cg···I)/Å | - | | - | 3.746 | 3.704 | 3.789 | 3.667 |
| $\nu$(OH) | | 3389 | | | | | |
| $\nu$(C=O)$^b$ or $\nu$(C=C)$^a$ | 1664 | | 1656 | 1672 | 1662 | 1670 | 1664 |
| $\nu$ ring$^i$ | | | 1633 | 1636 | 1623 | 1632 | 1621 |

| | | | | | | | |
|---|---|---|---|---|---|---|---|
| ν(C=C)$^{b,e}$ | 1542 | | 1525 | 1579 | 1582, 1551 | 1562 | 1587 |
| ν(C=O) + ν(C=C)$^g$ | | | 1527 | 1567 | 1506 | 1547 | 1560, 1521 |
| ν(C=C)$^{b,e,g}$ | | | 1486 | 1514, 1479 | | 1499 | 1438 |
| ν$_{as}$(C=C)$^e$ | | 1450 | | 1452 | | | |
| ν$_{as}$(C=C, aromatic)$^f$ | | | 1410 | 1428 | 1413 | 1428 | 1438 |
| ν(C-O) | | 1378 | | | | | |
| ν(C–C)$^{b,e}$ | | | 1360 | 1380, 1325 | 1346, 1317 | 1331 | 1345 |
| ν(C–C)$^b$ | 1248 | | 1278 | 1285 | 1256 | 1304 | 1264 |
| ν(C–C) + δ(OCC)$^d$ | 1176, 1169 | 1165 | | 1214 | 1206 | 1213 | 1203 |
| δ(C-H)$^f$ | | | 1190 | | | | |
| δ(O-H)$^h$ | | | | | | | |
| r(CH$_3$)$^g$ | 1040 | | 1092 | | | | |
| δ(C-C), ν (C-Cl)$^g$ | | | 1023 | 1051 | 1049 | 1054 | 1046 |
| ν(C–Br)+δ(OCC)$^d$ | 948 | 954 | 922 | | | | |
| δ(OCC)$^b$ | 707 | | 761 | 773 | 796 | 759 | 773 |
| ν(C–Br)$^g$ | 638 | 645 | 668, 648 | 694 | 671 | 690, 675 | 683, |
| δ(OH)$^h$ | | 606 | | | | | |

a Assignation according to Miller & Dixon, 1987;[35] b Assignation according to Boesch & Wheeler, 1997;[36] c Assignation according to Boesch & Wheeler, 1995;[37] d Assignation according to Zhang *et al.*, 2013;[38] e Our assignation according to our B3LYP calculations;[20] f *N*-MePy band, assignation according to Arenas *et al.*, 1996;[39] g Br$_4$Q$^-$ assignation, according to [6, 11]; h out of plane OH; i Cation in co-crystal

*DFT study of the charge transfer*

Quantum chemical modelling of intermolecular interactions with charge transfer is a rather complex issue, which is further complicated by the novelty of the studied systems. Therefore, elaborate quantum chemical computational study of the quinone-iodide co-crystals is a challenge on its own. Nevertheless, we present in this work results of selected theoretical treatments which point out to a partial charge transfer between the iodide and the quinone. The analysis is based on DFT calculations imposed both on the periodic solid state models, as well as on isolated clusters.

Bader charge analysis imposed on the electron density obtained by periodic DFT yields reliable estimate of charges contained within 'atomic' domains of the structure. Selected Bader charges of atoms and molecular/ionic entities are listed in Table 4.

**Table 4** Bader charges calculated from periodic models treated by the PBE DFT method and plane-wave basis set using the VASP package.

|  | $Br_4Q$ | $1_2 \cdot Br_4Q$ | $2_2 \cdot Br_4Q$ | $3_2 \cdot Br_4Q$ | $4_2 \cdot Br_4Q$ |
|---|---|---|---|---|---|
| C1 | +1.04 | +0.99 | +0.96 | +0.97 | +1.02 |
| C2 | -0.04 | +0.09 | -0.05 | -0.03 | -0.06 |
| C3 | -0.04 | -0.21 | -0.05 | -0.07 | -0.06 |
| O1 | -1.03 | -1.06 | -1.06 | -1.06 | -1.07 |
| Br1 | +0.04 | +0.01 | +0.02 | +0.01 | +0.01 |
| Br2 | +0.03 | +0.01 | 0.00 | 0.00 | +0.01 |
| total quinone | 0 | -0.35 | -0.36 | -0.35 | -0.28 |
| $I^-$ | - | -0.65 | -0.61 | -0.62 | -0.64 |
| total cation | - | +0.82 | +0.79 | +0.79 | +0.78 |

**Table 4** Cont'd

|  | $5_2 \cdot Br_4Q$ | $6_2 \cdot Br_4Q(1)^*$ | $6_2 \cdot Br_4Q(2)^*$ | $7_2 \cdot Br_4Q$ | $7_2 \cdot Cl_4Q$ |
|---|---|---|---|---|---|
| C1 | +1.01 | +0.98 | +0.97 | +0.98 | +0.98 |
| C2 | -0.08 | -0.10 | -0.06 | -0.10 | +0.11 |
| C3 | -0.10 | -0.02 | -0.08 | +0.01 | +0.14 |
| O1 | -1.05 | -1.04 | -1.03 | -1.06 | -1.07 |
| Br1/Cl1 | +0.01 | +0.02 | +0.02 | +0.01 | -0.15 |
| Br2/Cl2 | +0.01 | +0.02 | +0.03 | +0.02 | -0.16 |
| total quinone | -0.40 | -0.29 | -0.31 | -0.28 | -0.30 |
| $I^-$ | -0.61 | -0.62 | -0.62 | -0.61 | -0.60 |
| total cation | +0.81 | +0.77 | +0.77 | +0.75 | +0.75 |

\* $6_2 \cdot Br_4Q(1)$ – monoclinic form; $6_2 \cdot Br_4Q(2)$ – triclinic form.

The computed charges are quite consistent, so we may consider them as reliable. As expected, in the quinone molecule the most electron-depleted atom is C1 (carbonyl C), while the O1 is the electron-richest. The C=O bond is considerably polarized, but the negative charge accumulated on O1 slightly outweighs the positive charge on C1. In most cases, the same is true for the C—Br bonds; however, these are by far less polarized. As a result, in co-crystals the $Br_4Q$ molecules have a negative charge between -0.28 and -0.40, while the charge of the iodide anions is about -0.6 (or slightly above), which is considerably less than its formal charge of -1. At the same time, the charges accumulated on the cations (about +0.8) are also lower than the formal value of +1, indicating that the presently calculated degree of charge transfer may be overestimated. Experimentally determined charges of similar substituted *N*-methylpyridinium cations from our recent X-ray charge density studies of salts of $Cl_4Q$ radical anions[18,22] are very close to +1 (in fact, they all exceed +0.9); if we assume similar values for our crystals, the degree of charge transfer would be less than 5 %.

This is in agreement with observations: since the radical is a strong absorber of visible light, only a few percent of charge transfer would be enough to cause black color, while its impact on vibrational frequencies, chemical shifts and molecular geometry would still remain negligible or ambiguous. As recent results on halogen bonding show, a non-negligible degree of charge transfer is present even in interactions which are commonly believed to be purely electrostatic [40].

Worthy to note, the computed amount of charge transfer in $6_2 \cdot Br_4Q$ is barely different from other systems (Table 4), therefore the color difference between $6_2 \cdot Br_4Q$ (transparent) and other systems cannot be explained by the amount of charge located on entities forming the crystals; not at least on the basis of present calculations. Therefore we also considered the HOMO-LUMO gap, i.e. the energy required to promote the most excitable electron to the most stable vacant orbital; this quantity is indicative of light absorption properties of chemical systems. The HOMO-LUMO gap of a gas-phase cluster of $Br_4Q$ ($Cl_4Q$) and its six closest iodide neighbors extracted from crystal structures is listed in Table 5.

**Table 5** HOMO-LUMO gap (in a.u.) of an isolated cluster of quinone and its six closest iodide neighbors.

| compound | HOMO-LUMO gap |
|---|---|
| $1_2 \cdot Br_4Q$ | 0.139242 |
| $2_2 \cdot Br_4Q$ | 0.151254 |
| $3_2 \cdot Br_4Q$ | 0.147417 |
| $4_2 \cdot Br_4Q$ | 0.141963 |
| $5_2 \cdot Br_4Q$ | 0.146553 |

| | |
|---|---|
| **6**$_2$·Br$_4$Q(1)* | 0.099038 |
| **6**$_2$·Br$_4$Q(2)* | 0.107601 |
| **7**$_2$·Br$_4$Q | 0.148262 |
| **7**$_2$·Cl$_4$Q | 0.151681 |

* **6**$_2$·Br$_4$Q(1) – monoclinic form; **6**$_2$·Br$_4$Q(1) – triclinic form.

The HOMO-LUMO gap exhibits variations with the geometry of the polyhedron formed by iodide ions around the central Br$_4$Q (Cl$_4$Q) molecule. These variations are relatively small as long as the coordination of quinone remains the same (i.e. a quasi-octahedron in all cases but **6**$_2$·Br$_4$Q). For the latter however, the completely different arrangement of the neighboring iodide ions results in a substantially lower HOMO-LUMO gap which is by about 30% narrower than in other cases. Inspection of heterodimer clusters formed by one quinone molecule and one iodide ion reveals that the in-plane C—Br…I interactions contribute to significantly smaller HOMO-LUMO gaps than the interactions with the ring. While the presently computed HOMO-LUMO gaps cannot be used for quantitative prediction of the light absorption properties, let alone for the color of the crystals – the models lack the entire body of interactions actually present in the solid state – it is clear that in terms of light absorption compound **6**$_2$·Br$_4$Q is different from others, as reflected by the color of crystals.

Finally, we considered individual interactions between Br$_4$Q and the surrounding iodide ions. The pairwise interaction energies Br$_4$Q…I$^-$ mainly depend on the location of the iodide ion, and the in-plane I…Br(–C) interactions (estimated to 11-13 kcal/mol) are noticeably weaker than in the case where I$^-$ resides above the ring (17-19 kcal/mol). It should be noted however that the presently employed M06-2X functional yields unusually high energies of this interaction; the values obtained by the ab initio perturbational MP2 approach are lower by nearly one half

(between 6 and 10 kcal/mol). Having in mind that the interaction between iodide and quinone is to a large extent of dispersion nature, we feel that the MP2 approach yields more reasonable estimate of its energy. Nevertheless, regardless of the approach, the interaction appears to be strongest when iodide resides above the edge of the quinone ring (e.g., in $2_2 \cdot Br_4Q$) rather than above the center of the ring (e.g., in $1_2 \cdot Br_4Q$). The Natural Bond Orbital (NBO) analysis reveals that the in-plane interactions mainly involve electron lone pairs of iodide as the donating orbitals, and the C-Br antibond orbitals as acceptors, meaning that the attraction between iodide and bromine weakens the C-Br bonds; the effect increases on decreasing I…Br distance. On the other hand, when the iodide resides above the ring, its lone electron pairs tend to penetrate into the C=O and C=C antibond orbitals, thus facilitating charge transfer and affecting the π-system of quinone. As reflected in the interaction energies, the orbital interaction tends to be stronger when iodine is located above the edge of the quinoid ring (i.e. as close to the C=O and C=C bonds as possible).

The understanding of the iodide···quinone interaction poses a computational challenge on its own, therefore we plan to proceed in the future with advanced theoretical treatments, including superior electronic structure methodologies and energy decomposition analysis.


CONCLUSIONS

For the first time we have described anion···π contacts with quinoid rings, and have determined seven novel crystal structures with the I⁻···quinone···I⁻ unit; in addition there are two polymorphs of $6_2 \cdot Br_4Q$ where this unit is not present. According to color of the crystals, charge transfer between the iodide anion and the quinoid ring is expected; however according to solid-state

NMR and IR spectroscopies the interaction between the iodide anion and the quinoid ring is predominantly electrostatic, with a minor component of charge transfer. Preliminary computational study indicates that the interaction between the iodide and quinoid ring may be described as n → π* interaction which implies delocalization of a lone pair of the carbonyl or the iodide into an empty π* orbital of the quinone. To gain more insight into this unusual type of intermolecular interactions, more elaborate quantum chemical studies are in progress.

Charge transfer seems to be a more common phenomenon than previously believed: recent computational study of halogen bonding (which are generally believed to be electrostatic) found that the degree of charge transfer is non-negligible.[40] Therefore, we believe that a more detailed computational study will allow us to accurately assess the charge transfer.

The studied co-crystals may shed some light on the mechanism of reduction of the neutral quinones into their anion radicals.[41] The I⁻···quinone···I⁻ unit may be regarded as arrested reactions of reduction of the quinoid ring by the iodide anions. The closest contact between the iodide and the carbonyl carbon atom (> 3.52 Å) and n → π* donation indicate a possible mechanism of this reduction: a nucleophilic attack towards the carbonyl carbon. Another indication is prevalence of co-crystals with $Br_4Q$ *vs*. those with $Cl_4Q$ (7:1): more electronegative substituents stabilize the radical and facilitate reduction of the neutral quinone. Thus, $Br_4Q$, which reacts more slowly is more likely to form co-crystals, rather than radical salts.


EXPERIMENTAL

*Preparation*

Quinones and solvents used were purchased from commercial sources (Kemika Zagreb, Merck, Sigma-Aldrich) and were of p.a. grade. Iodide salts of *N*-methylated organic cations were

prepared by slowly adding a solution of methyl iodide in acetone (20 mmol in 10 mL) to an acetone solution of a corresponding organic base (20 mmol in 10 mL) with stirring. Crystalline solid started to precipitate almost immediately. After mixing of the reagents, the solutions were left to cool to 0 °C, then the *N*-methylated organic iodides were filtered and washed with cold acetone. Co-crystals of quinones and *N*-methylated organic iodides were prepared as described previously:[21] an excess of iodide salt was added to a saturated solution of a quinone in acetone. A reaction between neutral quinone and the iodide in the solution could be noted due to color change: the quinone is reduced to the radical anion, and the iodide to $I_2$ (indicated by dark brown color of the solution). However, instead of the radical salts, co-crystals of organic iodides with neutral quinones were formed. Dark red or black crystals would form within 2 - 3 hours. This may be a kinetically controlled process, since in some samples, upon standing in solution, crystals of semiquinone radical salt would start growing, and the iodide co-crystals would start to decompose.

*X-ray diffraction and refinement*

All structures were measured on an Oxford Diffraction Xcalibur Nova R (microfocus Cu tube). Program package CrysAlis PRO [42] was used for data reduction and multi-scan absorption correction. The structures were solved using SHELXS97 [43] and refined with SHELXL-2017.[43] The models were refined using the full-matrix least squares refinement; all non-hydrogen atoms were refined anisotropically. Hydrogen atoms bound to C atoms were modelled as riding entities using the AFIX command.

Molecular geometry calculations were performed by PLATON,[44] and molecular graphics were prepared using ORTEP-3,[45] and CCDC-Mercury.[46] Voronoi-Dirichlet polyhedra were drawn by

Topos PRO [47] and for calculation of Hirshfeld surfaces and electrostatic potential [DFT/B3LYP/6-311G(d,p)] was used Crystal Explorer 3.1.[48] Crystallographic and refinement data for the structures reported in this paper are shown in Table 6.

   Supplementary crystallographic data for this paper can be obtained free of charge via www.ccdc.cam.ac.uk/conts/retrieving.html (or from the Cambridge Crystallographic Data Centre, 12, Union Road, Cambridge CB2 1EZ, UK; fax: +44 1223 336033; or deposit@ccdc.cam.ac.uk). CCDC 1839281 – 1839290 contain the supplementary crystallographic data for this paper.

**Table 6** Crystallographic, data collection and structure refinement details.

| Compound | $1_2 \cdot Br_4Q$ | $2_2 \cdot Br_4Q$ | $3_2 \cdot Br_4Q$ | $4_2 \cdot Br_4Q$ |
|---|---|---|---|---|
| Empirical formula | $C_{10}H_{10}Br_2INO$ | $C_9H_9Br_2IN_2O$ | $C_{16}H_{14}Br_4I_2N_4O_2$ | $C_{11}H_{12}Br_2INO$ |
| Formula wt. / g mol$^{-1}$ | 446.91 | 447.90 | 867.71 | 460.94 |
| Crystal dimensions / mm | 0.15 x 0.12 x 0.10 | 0.20 x 0.12 x 0.09 | 0.19 x 0.11 x 0.10 | 0.15 x 0.15 x 0.15 |
| Space group | $P\,2_1/n$ | $P\,2_1/n$ | $P\,2_1/n$ | $P\,2_1/n$ |
| $a$ / Å | 7.7255(3) | 6.9830(2) | 7.35090(10) | 9.1002(1) |
| $b$ / Å | 12.2744(5) | 13.1092(4) | 11.9263(2) | 11.4827(2) |
| $c$ / Å | 14.0922(5) | 14.0234(4) | 13.9728(2) | 13.8538(2) |
| $\alpha$ / ° | 90 | 90 | 111.483(4) | 90 |
| $\beta$ / ° | 91.029(4) | 92.475(3) | 95.3900(10) | 91.5910(10) |

| | | | | |
|---|---|---|---|---|
| $\gamma$ / ° | 90 | 90 | 90 | 90 |
| $Z$ | 4 | 4 | 2 | 4 |
| $V$ / Å$^3$ | 1336.09(9) | 1282.53(6) | 1219.57(3) | 1447.09(4) |
| $D_{\text{calc}}$ / g cm$^{-3}$ | 2.222 | 2.320 | 2.366 | 2.116 |
| $\mu$ / mm$^{-1}$ | 25.652 | 26.749 | 28.100 | 23.709 |
| $\Theta$ range / ° | 4.78 – 76.39 | 4.62 – 75.69 | 4.88 – 75.67 | 5.00 – 75.82 |
| $T$ / K | 293(2) | 293(2) | 293(2) | 293(2) |
| Radiation wavelength | 1.54179 (Cu$K\alpha$) | 1.54179 (Cu$K\alpha$) | 1.54179 (Cu$K\alpha$) | 1.54179 (Cu$K\alpha$) |
| Diffractometer type | Xcalibur Nova | Xcalibur Nova | Xcalibur Nova | Xcalibur Nova |
| Range of $h$, $k$, $l$ | $-9 < h < 9$; | $-5 < h < 8$; | $-9 < h < 9$; | $-11 < h < 5$; |
| | $-15 < k < 14$; | $-16 < k < 16$; | $-12 < k < 14$; | $-13 < k < 14$; |
| | $-17 < l < 14$ | $-17 < l < 17$ | $-11 < l < 17$ | $-16 < l < 17$ |
| Reflections collected | 6819 | 6045 | 5947 | 4666 |
| Independent reflections | 2754 | 2627 | 2509 | 2977 |
| Observed reflections ($I \geq 2\sigma$) | 2427 | 2485 | 2467 | 2721 |
| Absorption correction | Multi-scan | Multi-scan | Multi-scan | Multi-scan |
| $R_{int}$ | 0.0500 | 0.0466 | 0.0304 | 0.0445 |
| $R\ (F)$ | 0.0887 | 0.0675 | 0.0424 | 0.0578 |
| $R_w\ (F^2)$ | 0.274 | 0.1842 | 0.1220 | 0.1672 |
| Goodness of fit | 1.069 | 1.064 | 1.051 | 1.049 |
| H atom treatment | Constrained | Constrained | Constrained | Constrained |
| No. of parameters | 138 | 136 | 127 | 145 |
| No. of restraints | 1 | 0 | 0 | 0 |
| $\Delta\rho_{max}$ , $\Delta\rho_{min}$ (eÅ$^{-3}$) | 2.543; -1.024 | 2.190; -2.741 | 1.809; -1.421 | 1.716; -1.497 |

**Table 5** Cont'd.

| Compound | $5_2 \cdot Br_4Q$, 100 K | $5_2 \cdot Br_4Q$, RT | $6_2 \cdot Br_4Q$, monoclinic | $6_2 \cdot Br_4Q$, triclinic |
|---|---|---|---|---|
| Empirical formula | $C_{24}H_{28}Br_4I_2N_2O_2$ | $C_{24}H_{28}Br_4I_2N_2O_2$ | $C_{11}H_{10}Br_2INO_3$ | $C_{11}H_{10}Br_2INO_3$ |
| Formula wt. / g mol$^{-1}$ | 949.92 | 949.92 | 490.92 | 490.92 |
| Crystal dimensions / mm | 0.15 x 0.12 x 0.10 | 0.15 x 0.08 x 0.06 | 0.20 x 0.15 x 0.14 | 0.10 x 0.08 x 0.6 |
| Space group | $P\,2_1/c$ | $P\,2_1/c$ | $P\,2_1/c$ | $P\,\bar{1}$ |
| $a$ / Å | 9.0199(2) | 9.0792(3) | 8.5556(1) | 7.8911(4) |
| $b$ / Å | 11.7488(3) | 11.9304(3) | 7.8155(1) | 8.3400(3) |
| $c$ / Å | 13.9845(4) | 14.1276(4) | 22.7206(2) | 11.6370(5) |
| $\alpha$ / ° | 90 | 90 | 90 | 97.364(3) |
| $\beta$ / ° | 102.981(3) | 103.421(3) | 99.959(1) | 100.646(4) |
| $\gamma$ / ° | 90 | 90 | 90 | 93.359(3) |
| Z | 2 | 2 | 4 | 2 |
| $V$ / Å$^3$ | 1444.11(6) | 1488.49(7) | 1496.35(3) | 743.80(6) |
| $D_{calc}$ / g cm$^{-3}$ | 2.185 | 2.119 | 2.179 | 2.192 |
| $\mu$ / mm$^{-1}$ | 23.784 | 23.074 | 23.091 | 23.227 |
| $\Theta$ range / ° | 4.97 – 75.65 | 4.91 – 75.93 | 3.95 – 76.03 | 3.90 – 75.86 |
| $T$ / K | 100(2) | 293(2) | 293(2) | 293(2) |
| Radiation vawelength | 1.54179 (Cu$K\alpha$) | 1.54179 (Cu$K\alpha$) | 1.54179 (Cu$K\alpha$) | 1.54179 (Cu$K\alpha$) |
| Diffractometer type | Xcalibur Nova | Xcalibur Nova | Xcalibur Nova | Xcalibur Nova |
| Range of $h$, $k$, $l$ | $-11 < h < 9$; | $-11 < h < 11$; | $-10 < h < 10$; | $-9 < h < 9$; |
|  | $-13 < k < 14$; | $-14 < k < 9$; | $-6 < k < 9$; | $-6 < k < 10$; |

|  | $-15 < l < 17$ | $-17 < l < 17$ | $-28 < l < 28$ | $-14 < l < 14$ |
|---|---|---|---|---|
| Reflections collected | 6932 | 5345 | 13970 | 6432 |
| Independent reflections | 2962 | 3069 | 3117 | 3051 |
| Observed reflections $(I \geq 2\sigma)$ | 2796 | 2876 | 2998 | 2873 |
| Absorption correction | Multi-scan | Multi-scan | Multi-scan | Multi-scan |
| $R_{int}$ | 0.0499 | 0.0378 | 0.0546 | 0.0480 |
| $R\ (F)$ | 0.0459 | 0.0575 | 0.0377 | 0.0486 |
| $R_w\ (F^2)$ | 0.1209 | 0.1786 | 0.1043 | 0.1421 |
| Goodness of fit | 1.038 | 1.078 | 0.985 | 0.890 |
| H atom treatment | Constrained | Constrained | Constrained | Constrained |
| No. of parameters | 155 | 156 | 163 | 164 |
| No. of restraints | 1 | 0 | 0 | 0 |
| $\Delta\rho_{max}$, $\Delta\rho_{min}$ ($e\text{Å}^{-3}$) | 2.097; -1.791 | 1.579; -2.937 | 0.824; -1.434 | 1.408; -1.776 |

**Table 5** Cont'd.

| Compound | **7₂**·Br₄Q | **7₂**·Cl₄Q |
|---|---|---|
| Empirical formula | $C_{12}H_9Br_2IN_2O$ | $C_{12}H_9Cl_2IN_2O$ |
| Formula wt. / g mol⁻¹ | 483.93 | 395.01 |
| Crystal dimensions / mm | 0.18 x 0.15 x 0.11 | 0.15 x 0.12 x 0.07 |
| Space group | $P\ 2_1/n$ | $P\ 2_1/n$ |
| $a$ / Å | 7.0071(3) | 6.925(5) |
| $b$ / Å | 14.7358(6) | 14.471(5) |
| $c$ / Å | 14.0153(5) | 13.695(5) |

| | | |
|---|---|---|
| $\alpha$ / ° | 90 | 90 |
| $\beta$ / ° | 96.498(4) | 97.578(5) |
| $\gamma$ / ° | 90 | 90 |
| Z | 4 | 4 |
| $V$ / Å$^3$ | 1437.86(10) | 1360.4(12) |
| $D_{calc}$ / g cm$^{-3}$ | 2.236 | 1.929 |
| $\mu$ / mm$^{-1}$ | 23.934 | 22.027 |
| $\Theta$ range / ° | 4.37 – 75.73 | 4.47 – 76.46 |
| $T$ / K | 293(2) | 293(2) |
| Radiation vawelength | 1.54179 (Cu$K\alpha$) | 1.54179 (Cu$K\alpha$) |
| Diffractometer type | Xcalibur Nova | Xcalibur Nova |
| Range of $h, k, l$ | $-8 < h < 8$; | $-8 < h < 8$; |
| | $-17 < k < 18$; | $-18 < k < 16$; |
| | $-10 < l < 17$ | $-17 < l < 17$ |
| Reflections collected | 7097 | 11515 |
| Independent reflections | 2948 | 2817 |
| Observed reflections ($I \geq 2\sigma$) | 2745 | 2587 |
| Absorption correction | Multi-scan | Multi-scan |
| $R_{int}$ | 0.0338 | 0.0772 |
| $R$ (F) | 0.0423 | 0.0499 |
| $R_w$ (F$^2$) | 0.1181 | 0.1419 |
| Goodness of fit | 1.064 | 1.097 |
| H atom treatment | Constrained | Constrained |
| No. of parameters | 163 | 163 |

| No. of restraints | 0 | 0 |
| $\Delta\rho_{max}$ , $\Delta\rho_{min}$ (eÅ$^{-3}$) | 1.199; -0.876 | 1.8; -1.192 |

*Solid-state NMR*

$^{13}$C magic-angle spinning (MAS) and $^{1}$H-$^{13}$C cross-polarization MAS (CPMAS) NMR measurements were carried out on a 600 MHz Varian NMR system equipped with a 3.2 mm Varian CPMAS probe. Larmor frequencies for $^{1}$H and $^{13}$C were 599.51 MHz and 150.75 MHz, respectively, and sample rotation frequency was 16 kHz. The CPMAS experiment employed RAMP [49] during the CP block with duration of 5 ms and high-power XiX [50] heteronuclear decoupling during acquisition; number of scans was 400 and repetition delay between scans was 30 s. In the MAS experiment, number of scans was 800 and repetition delay between scans was 100 s. Frequency axis of the $^{13}$C NMR spectra was referenced to tetramethylsilane.

*DFT computations*

First-principles calculations of isotropic chemical shifts of $^{13}$C nuclei were carried out with the GIPAW/DFT approach[51,52] using CASTEP software package (Materials Studio v. 5.5.3, Accelrys Software Inc.). Plane-wave basis, generalized gradient approximation of Perdew-Burke-Ernzerhof, and ultrasoft pseudopotentials (generated on-the-fly with CASTEP) were employed. Prior to GIPAW calculations, the structural models were optimized employing the DFT-based relaxation. Upon relaxation, force on each atom was smaller than 0.01 eV/Å and stress was below 0.02 GPa. In all calculations kinetic-energy cutoff for the plane-wave basis was set to 700 eV, and the reciprocal-space sampling was performed with the k-point grid spacing of 0.030 Å$^{-1}$

or less. GIPAW calculations yielded isotropic chemical shielding $\sigma^{\text{iso}}$, from which isotropic chemical shift was obtained as $\delta_{\text{CS}}^{\text{iso}} = 169 \text{ ppm} - \sigma^{\text{iso}}$.

Charge transfer between entities constituting the crystal structure was investigated by computing atomic charges using the established Bader population analysis [53] of the electron density. The density was computed by the program package VASP v. 5.3.5 [54-58], using the revised version [59] of the Perdew-Burke-Ernzerhof functional [60] corrected for dispersion interactions by the DFT-D3 method of Grimme *et al.* [61], Projector Augmented Wave atomic pseudopotentials [62], and a plane wave basis set with a kinetic energy cutoff of 500 eV. For each of the considered structures geometry optimization was performed, preserving the experimentally determined space group and keeping the unit cell parameters fixed. The integrals in the reciprocal space were computed on a Monkhorst-Pack $k$-point mesh [63] of sufficient density, such that the number of $k$-points in a given direction multiplied by the corresponding direct unit cell vector length exceeded 20 Å. Bader atomic charges of the computed density were calculated by scripts provided by the Henkelman group of the University of Texas at Austin [64-67].

Orbital interactions and the HOMO-LUMO gap were studied by isolated gas-phase cluster models consisting of one quinone molecule and up to 6 nearest iodide ions extracted from the experimental crystal structure of all the systems reported in the present study. For each of the models a single point calculation was performed, and was followed by the Natural Bond Orbital (NBO) analysis of the electronic structure [68], yielding the donor-acceptor stabilization energies between orbitals of the molecular entities included in the model. All gas-phase calculations were performed by the Gaussian09 program package [69] using the M06-2X density functional [70] coupled with the Dunning's valence double-zeta basis set [71], whereas the core electrons were

approximated by the Los Alamos pseudopotentials [72] (LANL2DZ). The use of pseudopotentials is mandatory due to the fact that the core part of the electronic structure of iodine exhibits sizable relativistic effects and is thus beyond the all-electron explicit treatment.

*IR spectroscopy*

Infrared spectra were measured on Vertex 80 (Bruker) by applying Golden Gate (Specac) diamond ATR equipment and MCT detector. The displacement of moving mirror was 0.25 that corresponds to a resolution of 4 cm$^{-1}$. Typically 64 scans were averaged. All spectra were recorded at room temperature.

ASSOCIATED CONTENT

Cif files, ORTEP drawings of quinones and cations, molecular geometries of the quinones, additional details of crystal packings, drawings of Voronoi-Dirichlet polyhedra, Hirshfeld surfaces with electrostatic potentials, solid-state NMR spectra, IR spectra.

AUTHOR INFORMATION

**Corresponding Author**

* K. Molčanov, e-mail: kmolcano@irb.hr

**Author Contributions**

The manuscript was written through contributions of all authors. All authors have given approval to the final version of the manuscript.

**Funding Sources**

**Notes**

Dedicated to prof. Dietmar Stalke on occasion of his 60th birthday.

ACKNOWLEDGMENT

ABBREVIATIONS

Cl4Q, tetrachloroquinone; Br4Q, tetrabromoquinone; VDP, Voronoi-Dirichlet polyhedra; HS, Hirshfeld surface.

REFERENCES

[1] Steed, J. W.; Atwood, J. L. (eds.) *Supramolecular Chemistry*, 2nd Ed., J. Wiley & Sons, Chichester, U.K., **2009**.

[2] Hunter, C. A.; Sanders, J. K. M. *The Nature of π-π Interactions*, *J. Am. Chem. Soc.* **1990**, *112*, 5525-5534.

[3] Hunter, C. A.; Lawson, K. R.; Perkins J.; Urch, C. J. *Aromatic Interactions*, *J. Chem. Soc., Perkin Trans. 2*, **2001**, 651-659.

[4] Salonen, L. M.; Ellermann M.; Diedrich, F. *Aromatic Rings in Chemical and Biological Recognition: Energetics and Structures*. *Angew. Chem., Int Ed.* **2011**, *50*, 4808-4842.

[5] Martinez, C. R.; Iverson, B. L. *Rethinking the term "pi-stacking"*, *Chem. Sci.*, **2012**, *3*, 2191-2201.

[6] Suezawa, H.; Ishihara, H.; Umezawa, Y.; Tsuboyama, S.; Nishio, M. *The Aromatic CH/π Hydrogen Bond as an Important Factor in Determining the Relative Stability of Diastereomeric Salts Relevant to Enantiomeric Resolution − A Crystallographic Database Study*, *Eur. J. Org. Chem.*, **2004**, 4816-4822.

[7] Nishio, M.; Hirota, M.; Umezawa, Y. *The C-H/π Interaction*, Wiley-VCH, New York, **1998**.

[8] Ma, J. C.; Dougherty, D. A. *The Cation-π Interaction*, *Chem. Rev.*, **1997**, *97*, 1303-1324.

[9] Schottel, B. L.; Chifotides, H. T.; Dunbar, K. R. *Anion-π interactions*, *Chem. Soc. Rev.*, **2008**, *37*, 68-83.

[10] a) Mooibroek, T. J.; Gamez, P.; Reedijk, J. *Lone pair–π interactions: a new supramolecular bond? CrystEngComm*, **2008**, *10*, 1501-1515; b) Frontera, A.; Gamez, P.; Mascal, M.; Mooibroek, T. J.; Reedijk, J. *Putting Anion-π Interactions Into Perspective*, *Angew. Chem., Int. Ed.*, **2011**, *50*, 9564-9583; c) Bauzá, A.; Mooibroek, T. J.; Frontera, A. *Towards design strategies for anion-π interactions in crystal engineering*, *CrystEngComm*, **2016**, *18*, 10-23.

[11] Wang, D.-X.; Wang, M.-X. *Anion-π interactions*. *J. Am. Chem. Soc.*, **2013**, *135*, 892-897.

[12] Singh, S. K.; Das, A. *The n → π\* interaction: a rapidly emerging non-covalent interaction*, *Phys. Chem. Chem. Phys.*, **2015**, *17*, 9596-9612.

[13] Lucas, X.; Bauzà, A.; Frontera, A.; Quiñonero, D. *A thorough anion–π interaction study in biomolecules: on the importance of cooperativity effects*, *Chem. Sci.*, **2016**, *7*, 1038-1050.

[14] Newberry, R. W.; Raines, R. T. *The n→π\* Interaction*, *Acc. Chem. Res.*, **2017**, *50*, 1838-1846; Singh, S. K.; Das, A. *The n→π\* interaction: A rapidly emerging non-covalent interaction. Phys. Chem. Chem. Phys.* 2015, **17**, 596-9612.

[15] Savastano, M.; Bazzicalupi, C.; Garcia, C.; Gellini, C.; López de la Torre, M. D.; Mariani, P.; Pichierri, F.; Bianchi, A.; Melguizo, M. *Iodide and triiodide anion complexes involving anion–π interactions with a tetrazine-based receptor*, *Dalton Trans.*, **2017**, *46*, 4518-4529.

[16] Echeverría, J. *Noncovalent Interactions in Succinic and Maleic Anhydride Derivatives*, *Cryst. Growth Des.* **2018**, *18*, 506-512.

[17] Molčanov, K.; Kojić-Prodić, B.; Babić, D.; Žilić, D.; Rakvin, B. *Stabilisation of tetrabromo- and tetrachlorosemiquinone (bromanil and chloranil) anion radicals in crystals*, *CrystEngComm*, **2011**, *13*, 5170-5178.

[18] Molčanov, K.; Jelsch, C.; Landeros-Rivera, B.; Hernández-Trujillo, J.; Wenger, E.; Stilinović, V.; Kojić-Prodić, B.; Escudero-Adán, A. *Partially covalent two-electron/multicentric bonding between semiquinone radicals*, submitted to *Cryst. Growth Des.*

[19] Molčanov, K.; Kojić-Prodić, B.; Babić, D.; Pajić, D.; Novosel, N.; Zadro, K. *Temperature induced reversible structural and magnetic phase transitions in a crystal of tetrachlorosemiquinone anion radical*, *CrystEngComm*, **2012**, *14*, 7958-7964.

[20] Molčanov, K.; Babić, D.; Kojić-Prodić, B.; Stare, J.; Maltar-Strmečki, N.; Androš, L. *Spin-coupling in dimers of 2,3-dicyano-5,6-dichlorosemiquinone radical anions in the crystalline state*, *Acta Crystallogr. B*, **2014**, *B70*, 181-190.

[21] Molčanov, K.; Stilinović, V.; Šantić, A.; Maltar-Strmečki, N.; Pajić, D.; Kojić-Prodić, B. *Fine tuning of π-stack separation distances of semiquinone radicals affects their magnetic and electric properties*, *Cryst. Growth Des.* **2016**, *16*, 4777-4782.

[22] Molčanov, K.; Mou, Z.; Kertesz, M.; Kojić-Prodić, B.; Stalke, D.; Demeshko, S.; Šantić, A.; Stilinović, V. *Pancake Bonding in π-Stacked Trimers in a Salt of Tetrachloroquinone Anion*, *Chem. Eur. J.*, **24** (2018), in print, DOI:10.1002/chem.201800672

[23] Molčanov, K.; Kojić-Prodić, B. *Spin pairing, electrostatic and dipolar interactions shape stacking of radical anions in alkali salts of 4,5-dichloro-3,6-dioxocyclohexa-1,4-diene-1,2-dicarbonitrile (DDQ)*. *CrystEngComm*, **2017**, *19*, 1801-1808.

[24] Molčanov, K.; Stalke, D.; Šantić, A.; Demeshko, S.; Stilinović, V.; Mou, Z.; Kertesz, M.; Kojić-Prodić, B. *Probing semiconductivity in crystals of stable semiquinone radicals: organic salts of 5,6-dichloro-2,3-dicyanosemiquinone (DDQ) radical anio*n. *CrystEngComm*, **2018**, *20*, 1862-1873.

[25] Molčanov, K.; Milašinović, V.; Stilinović, V.; Šantić, A.; Kojić-Prodić, B.; manuscript in preparation.

[26] Blatov, V. A. *Voronoi–dirichlet polyhedra in crystal chemistry: theory and applications*, *Crystallogr. Rev.*, **2004**, *10*, 249-318.

[27] Walsh, R. B.; Padgett, C. W.; Metrangolo, P.; Resnati, G.; Hanks, T. W. ; Pennington, W. T. *Crystal Engineering through Halogen Bonding: Complexes of Nitrogen Heterocycles with Organic Iodides*, *Cryst. Growth Des.* **2001**, *1*, 165-175.

[28] Stilinović, V.; Horvat, G.; Hrenar, T.; Nemec, V.; Cinčić, D. *Halogen and Hydrogen Bonding between (N-Halogeno)-succinimides and Pyridine Derivatives in Solution, the Solid State and In Silico*, *Chem. - Eur. J.*, **2017**, *23*, 5244-5257.

[29] Eraković, M.; Nemec, V.; Lež, T.; Porupski, I.; Stilinović, V.; Cinčić, D. *Halogen Bonding of N-Bromophthalimide by Grinding and Solution Crystallization*, *Cryst. Growth Des*. **2018**, *18*, 1182-1190.

[30] Ghassemzadeh, M.; Harms, K.; Dehnicke, K.; Fenske, D. *$\mu_2$-Halogenokomplexe von N-Bromsuccinimid und N-Bromphthalimid. Die Kristallstrukturen von PPh$_4$[X(N-Bromsuccinimid)$_2$] und von PPh$_4$[X(N-Bromphthalimid)$_2$] mit X = CI und Br*, *Z. Naturforsch. B* **1994**, *49*, 593-601.

[31] Nemec, V.; Lisac, K.; Stilinović, V.; Cinčić, D. *Inorganic bromine in organic molecular crystals: Database survey and four case studies*, *J. Mol. Struct.* **2017**, *1128*, 400-409.

[32] Kistenmacher, T. J.; Emge, T. J.; Bloch, A. N.; Cowan, D. O. *Structure of the red, semiconducting form of 4,4',5,5'-tetramethyl-[Delta]2,2'-bi-1,3-diselenole-7,7,8,8-tetracyano-p-quinodimethane, TMTSF-TCNQ, Acta Cryst. B*, **1982**, *B38*, 1193-1199.

[33] Girlando A.; Zanon I.; Bozio R.; Pecile C. *Raman and infrared frequency shifts proceeding from ionization of perhalo-p-benzoquinones to radical anions*, *J. Chem. Phys.* **1978**, *68*, 22-31.

[34] Puranik, M.; Chandrasekhar, J.; Snijders, J. G.; Umapathy, S. *Time-Resolved Resonance Raman and Density Functional Studies on the Ground State and Short-Lived Intermediates of Tetrabromo-p-benzoquinone*, *J. Phys. Chem. A*, **2001**, *105*, 10562-10569.

[35] Miller, J. S.; Dixon, D. A. *Dianion Stabilization by $(M(C_5(CH_3)_5)_2)^+$: Theoretical Evidence for a Localized Ring in $(DDQ)^{2-}$*, *Science*, **1987**, *235*, 871-873.

[36] Boesch, S. E.; Wheeler, R. A. *$\pi$-Donor Substituent Effects on Calculated Structures, Spin Properties, and Vibrations of Radical Anions of p-Chloranil, p-Fluoranil, and p-Benzoquinone*, *J. Phys. Chem. A*, **1997**, *101*, 8351-8359.

[37] Boesch, S. E.; Wheeler, R. A. *pi.-Donor Substituent Effects on Calculated Structures and Vibrational Frequencies of p-Benzoquinone*, *p*-Fluoranil, and *p*-Chloranil, *J. Phys. Chem.*, **1995**, *99*, 8125-8134.

[38] Wang, Y.; Zhang, F.; Ma, K.; Tang, G. *Experimental and DFT studies on the vibrational and electronic spectra of 2,3-dichloro-5,6-dicyano-1,4-benzoquinone*, *Spectrochim. Acta A*, 2**013**, *105*, 352-358.

[38] Arenas, J. F.; López Tocón, I.; Otero, J. C.; Marcos, J. I. *Vibrational spectrum of 2-methylpyridine*, *J. Mol. Struct.*, **1996**, *410-411*, 443-446.

[40] Thirman, J.; Engelage, E.; Huber, S. M.; Head-Gordon, M. *Characterizing the interplay of Pauli repulsion, electrostatics, dispersion and charge transfer in halogen bonding with energy decomposition analysis*, *Phys. Chem. Chem. Phys.* **2018**, *20*, 905-915.

[41] Bulfield, D.; Huber, S. M. *Halogen Bonding in Organic Synthesis and Organocatalysis*, *Chem. Eur. J.* **2016**, *22*, 14434-14450.

[42] *CrysAlis PRO*, Oxford Diffraction Ltd., U.K., **2007**.

[43] Sheldrick, G. M. *Crystal structure refinement with SHELXL*, *Acta Crystallogr. C*, **2015**, *C71*, 3-8.

[44] Spek, A. L. *Single-crystal structure validation with the program PLATON*, *J. Appl. Cryst.* **2003**, *36*, 7-13.

[45] Farrugia, L. J. *ORTEP-3* for Windows - a version of ORTEP-III with a Graphical User Interface (GUI), *J. Appl. Cryst.*, **1997**, *30*, 565.

[46] Macrae, C. F.; Edgington, P. R.; McCabe, P.; Pidcock, E.; Shields, G. P.; Taylor, R.; Towler, M.; van de Streek, J. *Mercury*: *visualization and analysis of crystal structures*, *J. Appl. Cryst.*, **2006**, *39*, 453-457.

[47] *Topos Pro, version 5.1.0.9*, Blatov, V. A.; Shevchenko, A. P. **2016**.; Blatov, V. A.; Shevchenko, A. P.; Proserpio, D. M. *Applied Topological Anaysis of Crystal Structures with the Program ToposPro*, *Cryst. Growth Des.* **2014**, *14*, 3576-3586.

[48] *CrystalExplorer (Version 3.1)*, Wolff, S. K.; Grimwood, D. J.; McKinnon, J. J.; Turner, M. J.; Jayatilaka, D.; Spackman, M. A. University of Western Australia, **2012**.

[49] Metz, G.; Wu, X. L.; Smith, S. O. J. *Ramped-Amplitude Cross Polarization in Magic-Angle-Spinning NMR, Magn. Reson. A* **1994**, *110*, 219-227.

[50] Detken, A.; Hardy, E. H.; Ernst, M.; Meier, B. H. *Simple and efficient decoupling in magic-angle spinning solid-state NMR: the XiX scheme, Chem. Phys. Lett.* **2002**, *356*, 298-304.

[51] Pickard, C.; Mauri, F. *All-electron magnetic response with pseudopotentials: NMR chemical shifts*, *Phys. Rev. B* **2001**, *63*, 245101.

[52] Yates, J.; Pickard, C.; Mauri, F. *Calculation of NMR chemical shifts for extended systems using ultrasoft pseudopotential*s, *Phys. Rev. B* **2007**, *76*, 024401.

[53] Bader, R. *A quantum theory of molecular structure and its application*s, *Chem. Rev.* **1991**, *91*, 893–928.

[54] Kresse, G.; Hafner J. *Ab initio Molecular-Dynamics for Liquid Metals*, *Phys. Rev. B* **1993**, *47*, 558–561.

[55] Kresse, G.; Hafner, J. *Ab-Initio Molecular-Dynamics Simulation of the Liquid-Metal Amorphous-Semiconductor Transition in Germanium*, *Phys. Rev. B* **1994**, *49*, 14251–14269.

[56] Kresse, G.; Furthmuller, J. *Efficient iterative schemes for ab initio total-energy calculations using a plane-wave basis set*, *Phys. Rev. B* **1996**, *54*, 11169–11186.

[57] Kresse, G.; Furthmuller, J. *Efficiency of ab-initio total energy calculations for metals and semiconductors using a plane-wave basis set*, *Comp. Mater. Sci.* **1996**, *6*, 15–50.

[58] Kresse, G; Hafner, J. *Norm-Conserving and Ultrasoft Pseudopotentials for First-Row and Transition-Elements*, *Phys. Condens. Mat.* **1994**, *6*, 8245–8257.

[59] Hammer, B.; Hansen, L. B.; Nørskov, J. K. *Improved adsorption energetics within density-functional theory using revised Perdew-Burke-Ernzerhof functionals*, *Phys. Rev. B*, **1999**, 59, 7413–7421.

[60] Perdew, J. P.; Burke, K.; Ernzerhof, M. *Local and gradient-corrected density functionals*, *Acs Sym. Ser.* **1996**, *629*, 453–462.

[61] Grimme, S.; Antony, J.; Ehrlich, S.; Krieg, H. *A consistent and accurate ab initio parametrization of density functional dispersion correction (DFT-D) for the 94 elements H-Pu*, *J. Chem. Phys.* **2010**, *132,* 154104.

[62] Kresse, G.; Joubert, D. *From ultrasoft pseudopotentials to the projector augmented-wave method*, *Phys. Rev. B* **1999**, *59*, 1758–1775.

[63] Monkhorst, H. J.; Pack, J. D. *Special Points for Brillouin-Zone Integrations*, *Phys. Rev. B* **1976**, *13*, 5188–5192.

[64] Tang, W.; Sanville, E.; Henkelman, G. *A grid-based Bader analysis algorithm without lattice bias*, *J. Phys. Condens. Matter* **2009**, *21*, 084204.

[65] Sanville, E.; Kenny, S. D.; Smith, R.; Henkelman, G. *An improved grid-based algorithm for Bader charge allocation*, *J. Comp. Chem.* **2007**, *28*, 899–908.

[66] Henkelman, G.; Arnaldsson, A.; Jónsson, H. *A fast and robust algorithm for Bader decomposition of charge density*, *Comput. Mater. Sci.* **2006**, *36*, 354–360.

[67] Yu, M.; Trinkle, D. R. *Accurate and efficient algorithm for Bader charge integration*, *J. Chem. Phys.* **2011**, *134*, 064111.

[68] Reed, A. E.; Curtiss, L. A.; Weinhold, F. *Intermolecular Interactions from a Natural Bond Orbital, Donor-Acceptor Viewpoint*, *Chem. Rev.* **1988**, *88*, 899–926.

[69] Frisch, M. J.; Trucks, G. W.; Schlegel, H. B.; Scuseria, G. E.; Robb, M. A.; Cheeseman, J. R.; Scalmani, G.; Barone, V.; B. Mennucci; Petersson, G. A.; Nakatsuji, H.; Caricato, M.; Li, X.; Hratchian, H. P.; Izmaylov, A. F.; Bloino, J.; Zheng, G.; Sonnenberg, J. L.; Hada, M.; Ehara, M.; Toyota, K.; Fukuda, R.; Hasegawa, J.; Ishida, M.; Nakajima, T.; Honda, Y.; Kitao, O.; Nakai, H.; Vreven, T.; J. A. Montgomery, J.; Peralta, J. E.; Ogliaro, F.; Bearpark, M.; Heyd, J. J.; Brothers, E.; Kudin, K. N.; Staroverov, V. N.; Kobayashi, R.; Normand, J.; Raghavachari, K.; Rendell, A.; Burant, J. C.; Iyengar, S. S.; Tomasi, J.; Cossi, M.; Rega, N.; Millam, J. M.; Klene, M.; Knox, J. E.; Cross, J. B.; Bakken, V.; Adamo, C.; Jaramillo, J.; Gomperts, R.; Stratmann, R. E.; Yazyev, O.; Austin, A. J.; Cammi, R.; Pomelli, C.; Ochterski, J. W.; Martin, R. L.; Morokuma, K.; Zakrzewski, V. G.; Voth, G. A.; Salvador, P.; Dannenberg, J. J.; Dapprich, S.; Daniels, A. D.; Farkas, O.; Foresman, J. B.; Ortiz, J. V.; Cioslowski, J.; Fox, D. J. *Gaussian 09*, Revision A.02; Gaussian, Inc.: Wallingford CT, 2009.

[70] Zhao, Y.; Truhlar, D. G. *The M06 suite of density functionals for main group thermochemistry, thermochemical kinetics, noncovalent interactions, excited states, and transition elements: two new functionals and systematic testing of four M06-class functionals and 12 other functionals*, *Theor. Chem. Acc.* **2008**, *120* 215–241.

[71] Dunning, T. H.; Hay, P. J. in *Modern Theoretical Chemistry*, Ed. H. F. Schaefer III, Vol. 3 (Plenum, New York, 1977) 1–28.

[72] Wadt, W. R; Hay, P. J. *Ab initio effective core potentials for molecular calculations – potentials for main group elements Na to Bi*, *J. Chem. Phys.* **1985**, *82,* 284–298.

For Table of Contents Use Only

Article Title

Iodide···π interactions of perhalogenated quinoid rings in co-crystals with organic bases*

Authors

Krešimir Molčanov, Gregor Mali, Jože Grdadolnik, Jernej Stare, Vladimir Stilinović, Biserka Kojić-Prodić

TOC graphic
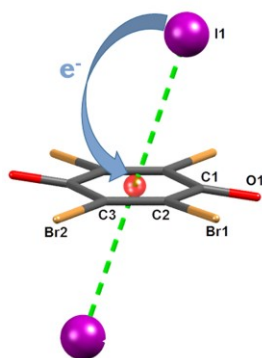


Synopsis

The first observed anion···π interactions involving a quinoid ring are described in a series of co-crystals of organic iodide salts and tetrahalogenquinones; black color of the crystals indicates charge transfer between iodide ions and quinoid rings.